Simulating photon pair generation in coupled lithium niobate nanowaveguides

Samuel Eserin

Department of Physics, University of Bath, Bath BA2 7AY, United Kingdom

Abstract. In this paper, we demonstrate theoretically, the design of a novel single photon source utilising the combined processes of second harmonic generation and non-degenerate parametric down conversion in two coupled X-cut lithium niobate nanowaveguides. Where highly frequency correlated photons are shown to be generated at wavelengths of 1620nm and 1405nm in the same spatial mode, with a purity of $P = 16.7\%$.

1. Introduction

1.1. Background

Single photons form the foundation of many emerging quantum technologies such as quantum simulation [1], quantum key distribution [2], quantum lithography [3] and quantum repeaters [4], that rely on utilising sources of single or entangled pairs of photons for their realisation. In particular, photonic quantum computing relies on highly efficient, scalable sources of high purity single photons for use as so called flying qubits [5].

Photons are an ideal candidate for quantum computing as they can operate under ambient conditions and readily satisfy the diVincenzo criteria [6], a set of criteria that must be fulfilled for the successful construction of a quantum computer. Additionally, they can travel long distances down optical fibres without interacting, making them ideally suited to quantum key distribution. One key approach to the generation of single photons, has been the use of spontaneous four wave mixing in materials such a silica, with the required $\chi^{(3)}$ non-linearity [7, 8]. However, exploiting the stronger $\chi^{(2)}$ non-linearity of lithium niobate compared to $\chi^{(3)}$ of silicon allows for lower pump powers to be used, and helps avoid unwanted non-linear effects such as Raman scattering and self-phase modulation which would limit photon purity. Additionally, on-chip integration of a photon source and a detector requires the removal of unwanted pump field from the generated photons, which is difficult to achieve with photons generated through four wave mixing processes due to a small spectral separation between the pump and generated wavelengths [9].

Heralded single photon sources based on spontaneous parametric down conversion (SPDC) [10] provide an alternative approach. Here, a single pump photon has a probability of spontaneously being converted into a pair of photons at longer wavelengths, termed the signal and the idler, where the idler is then detected to herald the presence of it's twin [11]. Second order non-linear processes, such as SPDC, occur as a result of the interaction between a photon and the medium in which it is propagating, if, and only if the crystal is noncentrosymmetric and therefore lacks inversion symmetry [12]. Lithium niobate, and specifically thin film lithium niobate on insulator, has been a popular choice of material for such applications due to its strong $\chi^{(2)}$ non-linear coefficients [13], opto-electrical properties [14] and the ability to exploit the pre-existing manufacturing infrastructure already present for silicon photonics [15], therefore making it an ideal candidate for photonically integrated circuits [16]. Lithium niobate simultaneously allows for periodic domain inversion which has seen wide spread use in periodically polled lithium niobate (PPLN) waveguiding structures [17]. Periodically polled lithium niobate is a key example of utilising quasi-phasematching for application

in single photon schemes, where it has been used to achieve a photon purity of 64% and conversion efficiencies of 4×10^{-6} [18]. Periodic polling has also been used in periodically polled KTP, where a single photon yield of $> 90\%$ and a photon purity of 99% was reported [19]. The drawback to periodically polling is primarily the expensive fabrication techniques required to create this array of domains.

The approach presented here offers an elegant alternative to achieving photon pair generation by utilising the combined processes of second harmonic generation (SHG) and spontaneous parametric down conversion (SPDC) in two coupled waveguides. The benefits of using two coupled waveguides are three-fold: by utilising the process of second harmonic generation in waveguide 1, we remove the need to pump directly at about $750nm$ in a higher order mode, which would be experimentally challenging and which would be necessary if using a single waveguide. Secondly, we can more easily separate pump photons from the generated photon pairs. This would allow for us to avoid filtering at a later date (which could reduce visibility), and also allows for more feasible integration of source and detector for integrated on-chip design. Finally, by ensuring that the waveguides are of different geometries, we can minimise the coupling of our generated signal and idler back into waveguide 1, ensuring that they remain guided in the waveguide in which they are generated.

1.2. Second order nonlinear processes

Nonlinear optics is the study of the phenomena whereby the spectral content of a high power laser pulse is modified through interaction with a particular medium. This can be seen by looking at the dependence of the material polarisation on the presence of an electric field. Polarisation of a medium can be considered as a delayed response of electric dipoles within the medium to the presence of an electric field [12]. In this study, it is sufficient to only consider the second order non-linear effects, since we are interested in the processes of second harmonic generation and spontaneous parametric down conversion, shown schematically in Fig. 1.

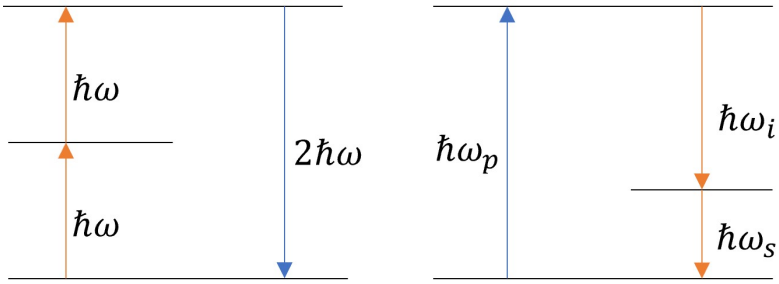

Figure 1: A schematic showing the photon energy transitions involved in the SHG (left) and SPDC (right) processes.

Second harmonic generation can be thought of as the response of a medium to a driving electric field of frequency ω, causing oscillations of the dipoles within the material at frequencies ω and 2ω, thus leading to re-emission at these frequencies. Quantum mechanically, this process can be visualised as the combination of two photons at frequency ω, to form a single photon at twice this frequency. During this study, SHG is utilised to generate an oscillating pump field with desirable properties which will then be coupled to a complementary parametric down conversion process. Spontaneous parametric down conversion involves the probabilistic decomposition of a single pump photon into two daughter photons, termed the "signal" and the "idler" and in the degenerate case can be considered as the time reversed process of second harmonic generation. In both processes energy is necessarily conserved:

$$\hbar\omega_p = \hbar\omega_s + \hbar\omega_i \tag{1}$$

where $\hbar$ is Plank's constant and $\omega_{p,s,i}$ are the frequencies of pump, signal and idler respectively. The propagation constant of a given mode, m is defined as

$$\beta_m(\omega) = \omega n_{eff,m}(\omega)/c \tag{2}$$

where m can be any of the pump, signal or idler modes and c is the speed of light in a vacuum. This allows us to define a phase mismatch parameter:

$$\Delta\beta = \beta_p - \beta_s - \beta_i \tag{3}$$

which is the difference in the propagation constants of pump, signal and idler, and the condition $\Delta\beta = 0$ corresponds to a conservation of linear momentum where both SHG and SPDC processes are optimised. This condition is referred to as phasematching.

Phasematching is typically achieved through birefringent or quasi - phasematching. Birefringent phasematching occurs when variations in the waveguide geometry allow for the agreement of polarisation dependent refractive indices of the modes of interest. Quasi-phasematching is achieved by periodically reversing the polarisation of the material (sign of $\chi^{(2)}$) to offset the periodic phase mismatch, where the wavevector associated with the periodic crystal domain reversal allows for momentum conservation, and has seen widespread use in lithium niobate structures. Here we use a third method, whereby we select a combination of different waveguide modes which allow for phasematching to be upheld.

1.3. Dual waveguide approach

A schematic for the modelled system is presented in Fig. 2. Laser light is incident on the first waveguide, in which second harmonic generation takes place. After generating a second harmonic field in waveguide 1, it is then coupled to a corresponding higher order mode in waveguide 2, where it acts as a pump field for the SPDC process to take place. To obtain coupling between two higher order modes in the neighbouring waveguides it is desirable for them to have matching wavelengths and effective indices. It is also desirable for the higher order modes in both waveguides to have the same polarisation, however, this is not essential as coupling will take place regardless. The geometry of the second waveguide is such that exact phasematching occurs between a higher order mode and a single fundamental mode, in which photons are generated through SPDC, however, it is noted that it is unlikely that exact phasematching can be simultaneously achieved for SHG in waveguide 1.

2. Results

2.1. Coupled waveguide system

In order to determine the properties of the pump mode which is to be generated via SHG in waveguide 1, the first step was to study the SPDC in waveguide 2. As a starting point, the geometry detailed in [20] is used, as phasematching is known for this geometry for the generation of photons at around $1550nm$. However, this geometry differs from that presented here primarily due to the presence of a residual thin film of lithium niobate. This is a useful parameter to retain within the structure as it provides an additional parameter for optimisation. For this initial geometry, suitable modes were determined through mode analysis studies within the finite element method solver COMSOL Multiphysics. These studies allowed for the effective refractive index of appropriate modes to be plotted as a function of wavelength as shown in Fig. 3. The crossing point between modes indicates the point at which phasematching takes place ($\Delta\beta = 0$ in Eq. (3)). This phasematching point indicates the wavelength at which degenerate photon pairs are produced through SPDC and occurs for a wavelength of about $1520nm$. For this to occur a pump wavelength of $760nm$ is required. It is noted here that for the wavelength range being studied, no other pump modes are phasematched with the signal/idler mode and are therefore ignored.

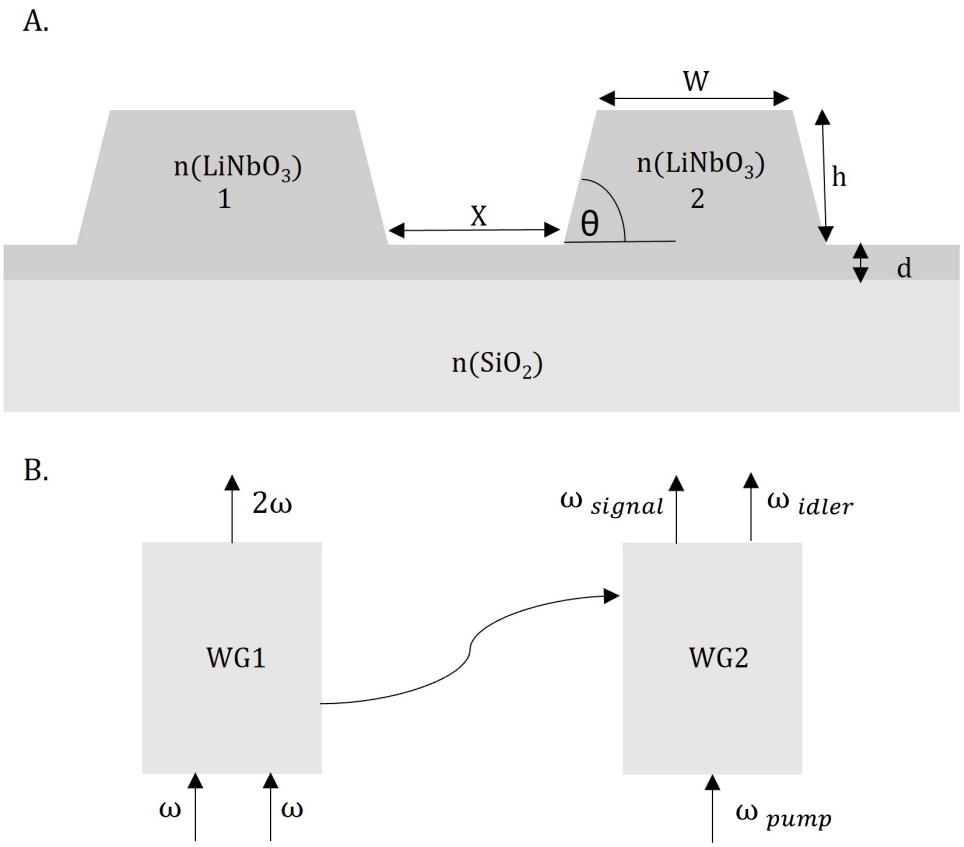

Figure 2: (A). The design of the dual waveguide setup simulated during this work, X=waveguide separation, h=waveguide height, d=residual film height, W=waveguide top width and θ=side wall angle. Waveguides 1 and 2 are indicated accordingly. (B). A top down view of the two waveguides, showing the SHG process occurring in waveguide 1 (WG1) and the SPDC process in waveguide 2 (WG2), the arrow moving between the waveguides indicates coupling of the photons generated through SHG in WG1 into WG2.

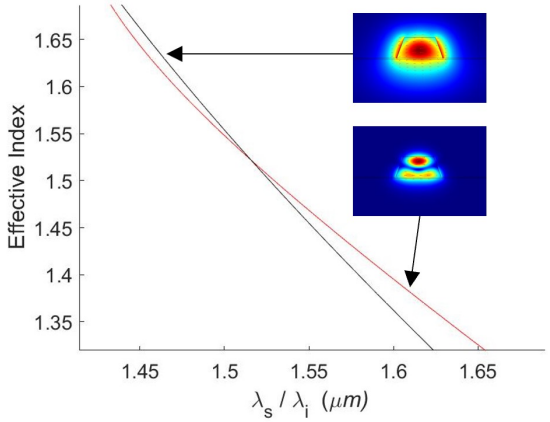

Figure 3: Effective refractive index is plotted as a function of wavelength for two modes within the waveguide 2 structure with $W = 500nm$, $h = 330nm$, $d = 20nm$ and $\theta = 70°$. A higher order pump mode is indicated in red and the fundamental mode into which the signal and idler photons are generated is shown in black, exact phasematching occurs at the wavelength of crossing between the modes. Mode profiles label their respective modes. Here the higher order mode (red) is plotted for wavelengths $\lambda_s/2$.

A key component of this work is the characterisation of the spectral content of the generated signal and idler photons. This is achieved through the calculation of their joint spectral amplitude and the plotting of their joint spectral intensity.

The wavefunction for the generated photons in the SPDC process can be described using a two-photon state function [21]:

$$|\psi_2\rangle \;=\; \int\int d\omega_s d\omega_i \alpha(\omega_s+\omega_i)\Phi(\omega_s,\omega_i)\;|\omega_s\rangle\;|\omega_i\rangle \tag{4}$$

where $\alpha(\omega_s+\omega_i)$ is the pump envelope function for which a Gaussian is initially assumed:

$$\alpha(\omega_s+\omega_i) = \;exp\left\{\frac{(\omega_p\;-\;\omega_s\;-\;\omega_i)^2\,t_0^2}{2}\right\} \tag{5}$$

This approximation is only used to generate the plots in Fig. 4, later on, the full dependency of the pump envelope function on ω and z - the distance down the waveguide - will be used. The pump envelope function and determines the range of pump frequencies which can be used in down conversion, $\omega_{p,s,i}$ are the pump, signal and idler frequencies respectively and t_0 is the pulse duration. $\Phi(\omega_s,\omega_i)$ in Eq. (5) is the phasematching function, which determines the distribution of pump energies into signal and idler photons:

$$\Phi(\omega_s,\omega_i\;) = \;\int_0^L \rho_2\;\exp\{i\Delta\beta\;z\}\;dz \tag{6}$$

Performing this integral yields a phasematching function with distinctive sinc profile shown in Fig. 4, where the maxima of this phasematching function correspond to $\Delta\beta(\omega_s,\omega_i,u)=0$. ρ_2 is the nonlinear coefficient, and is constant along L, the length of the waveguide. Following this, we can define the joint spectral amplitude, the probability amplitude of each pair of generated photons, as the product $\alpha(\omega_s+\omega_i)\Phi(\omega_s,\omega_i)$ in Eq. (5)

$$J(\omega_s,\omega_i) \;=\; \rho_2 exp\left\{\frac{(\omega_p\;-\;\omega_s\;-\;\omega_i)^2\,t_0^2}{2}\right\} sinc\left[\frac{\Delta\beta L}{2}\right] exp\left\{i\frac{\Delta\beta L}{2}\right\} \tag{7}$$

where the corresponding joint spectral intensity is given by $JSI = |(J)|^2$. A comprehensive background to the description presented here can be found in [21–24].

The corresponding phasematching function for this geometry is shown on the LHS of Fig. 4. Initially, it is assumed that the higher order pump mode is approximately Gaussian in profile and has no dependency along the propagation dimension of the waveguide. This approximation is used to characterise the joint spectral intensity of the photons generated through SPDC in waveguide 2, shown on the RHS of Fig. 4. However, this approximation is later abandoned in favour of a more accurate pump spectral amplitude and phasematching, based on the fixed geometries of both waveguides and accounting for coupling between them. It can be seen in the plot of the phasematching function, that by detuning from a pump wavelength of $760nm$ (yielding degenerate photon pair production) to a wavelength of $752nm$, that the point at which overlap occurs between our pump function and our phasematching function is shifted. As a consequence of this, non-degenerate photons are now generated at wavelengths of about $1620nm$ and $1405nm$, indicated by the corresponding joint spectrum.

Detuning in this way fixes the pump wavelength required to generate photons at the wavelengths given by the joint spectrum. Consequently, the effective refractive index of the higher order mode at this wavelength can then be determined. At a wavelength of $\lambda_p = 0.752nm$ this higher order mode has an effective index $n_{eff} = 1.5269$. To ensure coupling between the two waveguides, this higher order mode in waveguide 2 must be matched in wavelength and effective refractive index to a higher order mode in waveguide 1 - which is generated through second harmonic generation. Thus by detuning

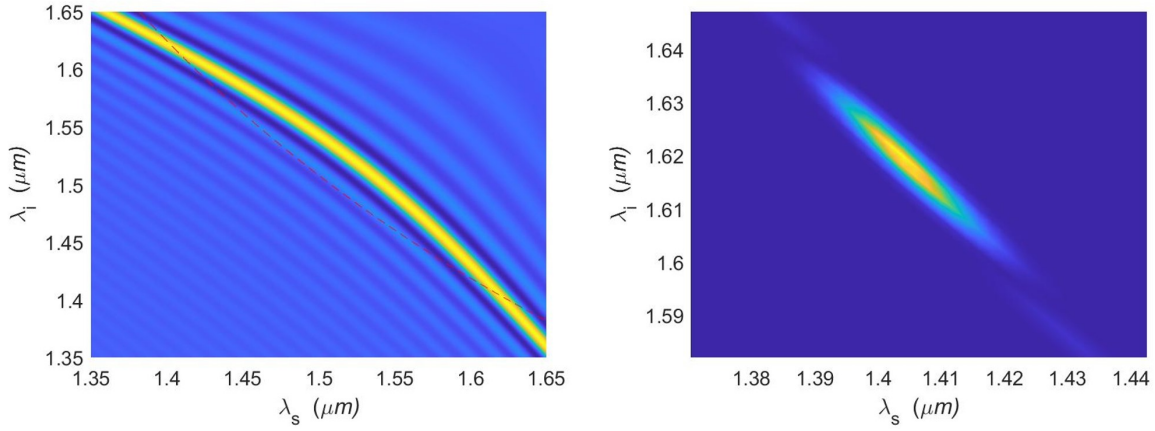

Figure 4: Phasematching function (left) with red dashed line indicating the approximated Gaussian field envelope of the pump pulse and corresponding JSI (right). Here the waveguide length $L = 1000\mu m$ and the initial pulse duration $t_0 = 2ps$.

to a wavelength of $\lambda_p = 0.752nm$ and effective refractive index of $n_{eff} = 1.5269$, we determine the effective refractive index of the higher order mode in waveguide 1 and its wavelength. The geometry of waveguide 1 can then be determined by searching for a geometry where a higher order mode with this wavelength and effective index exists.

Due to restrictions imposed by the manufacturing process [15], all geometrical parameters, besides the top width, must be the same for both waveguides, and therefore $h = 330nm$, $d = 20nm$ and $\theta = 70°$ are fixed from this point on. This leaves the waveguide top width as the only variable parameter in the search for a second dissimilar waveguide geometry for waveguide 1, in which we search for a higher order mode guided at $\lambda_p = 0.752nm$ with an effective refractive index of $n_{eff} = 1.5269$. Potential geometries for waveguide 1 were found by fixing the wavelength at $\lambda_p = 0.752nm$ and looking at how the effective index varied as a function of waveguide top width for a number of possible higher order modes within the waveguide.The resulting plot is shown in Fig. 5.

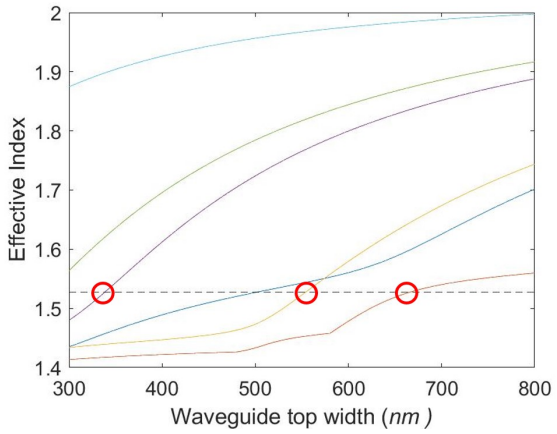

Figure 5: Variation in the effective mode index of 6 modes of interest within waveguide 1. The black dashed line indicates an effective mode index of $n_{eff} = 1.5269$. Crossing points with this dashed line indicate possible widths, where it is noted that the mode in blue corresponds to our waveguide 2 top width and since we desire dissimilar waveguides, this solution is ignored. Solutions circled in red are those which are considered further.

As is indicated by the intersection of the curves with the dashed black line, for several modes there is a width for which that mode has an effective refractive index which matches that of the pump mode

in waveguide 2, this gives three possible solutions for the top width of waveguide 1. Each is explored in turn, and the chosen solution is that for which there is the closest agreement in effective refractive index between the higher order mode and one of the guided fundamental modes in waveguide 1. This is necessary since input laser light will propagate in a fundamental mode in waveguide 1. It was determined through mode analysis studies that for waveguide 1, a top width of $W = 664nm$ showed the closest agreement in effective refractive indices to a corresponding fundamental mode. These modes are detailed in Fig. 6. Selecting these modes, fixes our top width of waveguide 1 at $W = 664nm$ and therefore both geometries are now fixed. It is also noted that due to energy conservation, the laser used to generate photons through SHG in waveguide 1 has a corresponding wavelength of $\lambda = 1504nm$.

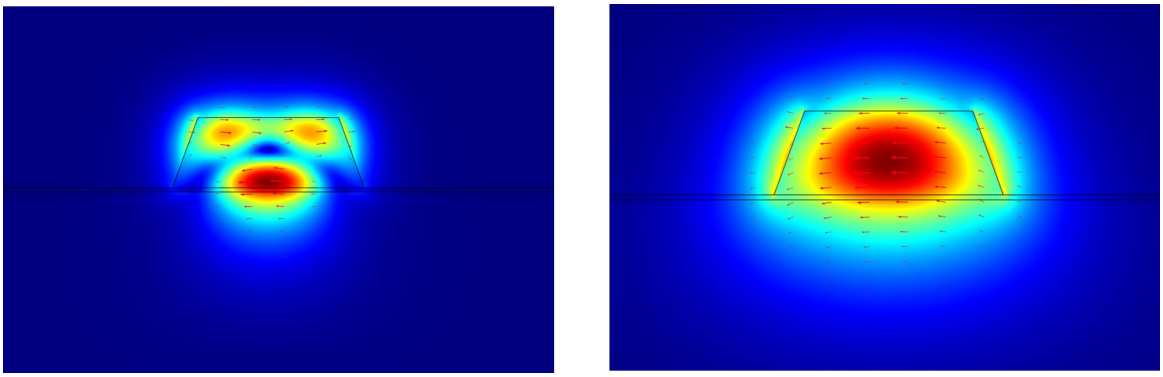

Figure 6: Mode profiles in waveguide 1. The higher order mode (left), $neff = 1.5269$ at $\lambda = 752nm$. The fundamental mode (right) $neff = 1.6119$ at $\lambda = 1504nm$.

Additionally, a model for the combined waveguide system was developed within COMSOL Multiphysics where the symmetric and anti symmetric supermodes for the structure are shown in Fig. 7. Coupled mode theory allows for the separation in effective mode index of these supermodes to be related to the coupling constant, C of the system, a measure of the coupling strength between the two waveguides.

$$C = \frac{\beta(symmetric) - \beta(antisymmetric)}{2} \tag{8}$$

It is well known that the coupling constant decays off exponentially as the separation between the waveguides is increased and as such, an exponential decay can be fitted to the obtained coupling constant data. This allows us to vary the coupling constant directly to any desired value when fine tuning the structure, by changing the separation between the waveguides.

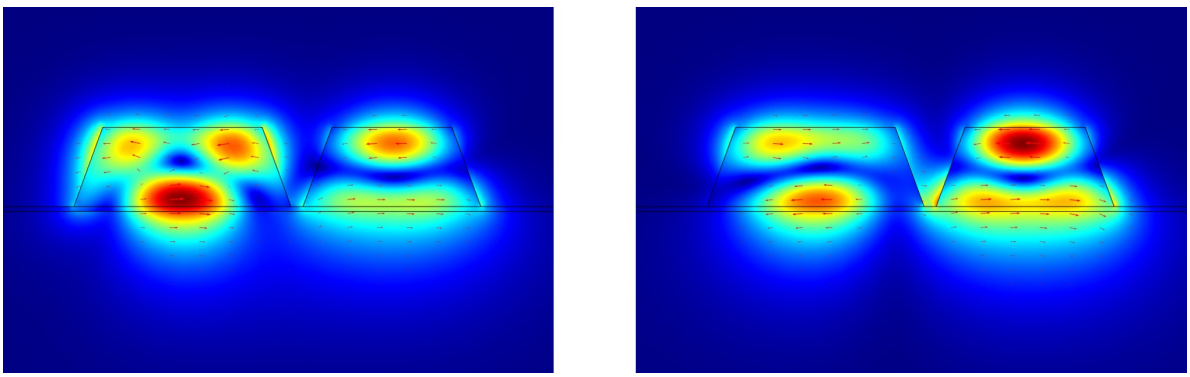

Figure 7: Supermode profiles for the antisymmetric (left) and symmetric (right) modes in the combined waveguide geometry.

It is important to have a direct measure of the coupling constant for the system as this appears directly in the field evolution equations used to describe our system. Solving the field evolution equations allows for us to find a solution for the second harmonic propagating in waveguide 2, and thus to obtain a more precise pump envelope function. Consequently, we can re-calculate a joint spectrum based on the pump function generated through our setup.

2.2. Field evolution equations

Here the mathematical model presented is an adaptation of that used in [20], where we consider two coupled waveguides, invariant along the direction of propagation, and thus have a third field. Here, we also account for the coupling between the two waveguides. The propagation constants, β, group velocities, $v_g = (\beta_1)^{-1}$ and group velocity dispersions, β_2 are determined for the fundamental mode and the second harmonic in waveguide 1 and the second harmonic in waveguide 2. Where, β is calculated according to Eq. (3), $\beta_1 = d\beta/d\omega$ and $\beta_2 = d^2\beta/d\omega^2$. Eqs. (9-11), describe the evolution of the field envelopes of three light fields; the fundamental field in waveguide 1, $U_f(z,t)$, the second harmonic generated through SHG, $U_s(z,t)$, and the higher order mode in waveguide 2, $U_p(z,t)$, which forms our updated pump envelope function.

$$i\frac{\partial U_f}{\partial \xi} = -r_2\frac{\partial^2 U_f}{\partial \tau^2} - U_f^* U_s e^{i\kappa\xi} \tag{9}$$

$$i\frac{\partial U_s}{\partial \xi} = -s_1 i\frac{\partial U_s}{\partial \tau} - s_2\frac{\partial^2 U_s}{\partial \tau^2} - \frac{1}{2U_f^2}e^{(-i\kappa\xi)} + CU_p \tag{10}$$

$$i\frac{\partial U_p}{\partial \xi} = -p_1 i\frac{\partial U_p}{\partial \tau} - p_2\frac{\partial^2 U_p}{\partial \tau^2} + CU_s \tag{11}$$

Where in these equations, t has been shifted such that we are in the reference frame of the fundamental field propagating in waveguide 1, $\tau = t/t_0 - z_d\beta_{f1}\xi/t_0$ and z has been normalised by the dispersion length $z_d = 2t_0^2/|\beta_{f2}|$ to give a normalised distance $\xi = z/z_d$. C is the coupling constant for a given separation and κ is the phase mismatch $\kappa = \Delta\beta z_d$. The remaining coefficients are defined as follows:

$$z_{w(s,p)} = \frac{t_0}{\beta_{s1,p1} - \beta_{f1}} \qquad r_2 = -1$$

$$s_1 = \frac{z_d}{z_{ws}} = \frac{2t_0\left(\beta_{s1} - \beta_{f1}\right)}{|\beta_{f2}|} \qquad s_2 = \frac{-z_d\beta_{s2}}{2t_0^2} = \frac{-\beta_{s2}}{|\beta_{f2}|}$$

$$p_1 = \frac{z_d}{z_{wp}} = \frac{2t_0\left(\beta_{p1} - \beta_{f1}\right)}{|\beta_{f2}|} \qquad p_2 = \frac{-z_d\beta_{p2}}{2t_0^2} = \frac{-\beta_{p2}}{|\beta_{f2}|}$$

The values for $\beta_{f,s,p}$, $\beta_{1,f,s,p}$ and $\beta_{2,f,s,p}$ are calculated previously for the modes of interest within our geometry. Where, f, s, p correspond to the fundamental in waveguide 1, second harmonic in waveguide 1 and pump in waveguide 2 respectively. Eqs. (9-11), are solved in the frequency domain via performing the appropriate Fourier transforms, such that the resulting pump function $\tilde{U}_p(\xi,\omega)$ is a function of frequency as required.

$$\frac{\partial \tilde{U}_f}{\partial \xi} = -ir_2\omega^2\tilde{U}_f + i\mathcal{F}(U_f^* U_s e^{i\kappa\xi}) \tag{12}$$

$$\frac{\partial \tilde{U}_s}{\partial \xi} = -i(s_1\omega + s_2\omega^2)\tilde{U}_s + i\mathcal{F}(\frac{1}{2}U_f^2 e^{-i\kappa\xi}) - iC\tilde{U}p \tag{13}$$

$$\frac{\partial \tilde{U}_p}{\partial \xi} = -i(p_1\omega + p_2\omega^2)\tilde{U}_p - iC\tilde{U}_s \tag{14}$$

The field evolution equations can be solved by taking Fourier transforms and then solving the resulting coupled ordinary differential equations. This reduces down to solving an initial value problem, with solutions to the coupled ODE's which are the field profiles $\tilde{U}_f$, $\tilde{U}_s$, $\tilde{U}_p$ as functions of frequency and normalised distance along the waveguide. Initially, $\tilde{U}_f$ is considered to be a Gaussian laser pulse and there is no intensity in either of the $\tilde{U}_s$ or $\tilde{U}_p$ fields. The solutions $\tilde{U}_s$ and $\tilde{U}_p$ are shown in Fig. 8. Where the solution $\tilde{U}_p$ is our revised pump function in waveguide 2.

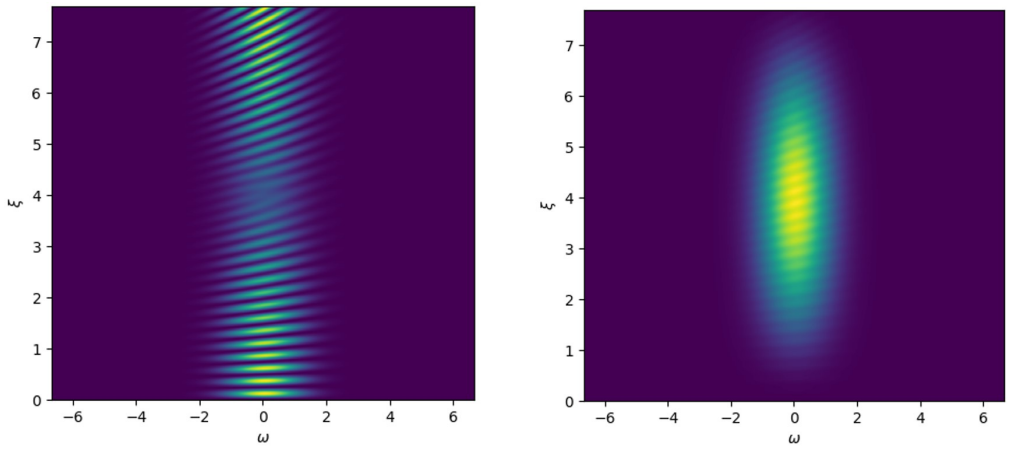

Figure 8: Field distributions for the second harmonic in waveguide 1 (left) and waveguide 2 (right) plotted in frequency, ω and normalised distance, ξ. For a pulse duration $t_0 = 7ps$, a waveguide length, $L = 9000\mu m$ and a waveguide separation, $X = 420nm$.

For the purposes of this devices design, it is desirable, for any length of waveguide, to have only one full oscillation in the pump field of waveguide 2, $\tilde{U}_p$, such that there is only a single down conversion process taking time per pulse of laser light. Additionally, we want to increase the length of the waveguide such that the width of the phasematching function is narrowed. To increase the length but still retain a single full oscillation in $\tilde{U}_p$, the coupling constant is tuned for each length by increasing the separation as length increases. Changing the coupling constant for a fixed length will vary the distance in ξ between sequential oscillations of $\tilde{U}_p$, a larger coupling constant leads to shorter distances in ξ between neighbouring oscillations. By fixing the length of the waveguide such that the bandwidth of the phasematching function is sufficiently narrow, and then tuning the coupling constant accordingly, it is possible to then use the solution $\tilde{U}_p$ as our revised pump envelope function. This allows for the more accurate determination of the Joint spectrum based specifically on our new pump envelope function, shown in Fig. 8. The revised joint spectrum is calculated using

$$J(\omega_p) \;=\; \int_0^L \tilde{U}_p(\omega_p, z) exp\left\{ i\frac{\Delta\beta z}{2} \right\} dz \tag{15}$$

Where L is the length of the device and the pump function is explicitly written in terms of the signal and idler frequencies $\tilde{U}_p(\omega_p, \xi) = \tilde{U}_p(\omega_i, \omega_s, \xi)$. The resulting joint spectral intensity $JSI = |(J(\omega_p))|^2$ for an initial pulse duration $t_0 = 7ps$, a waveguide length of $L = 9000\mu m$ and a waveguide separation of $X = 420nm$ is presented in Fig. 9.

2.3. Photon Purity

Now that a more accurate joint spectrum has been obtained, we can study the degree of correlation between the signal and idler photons and extract the photon purity. This is achieved by expressing the joint spectrum as the sum of orthogonal modes, performing the singular valued decomposition of the JSA and analysing the photon purity using the expansion coefficients:

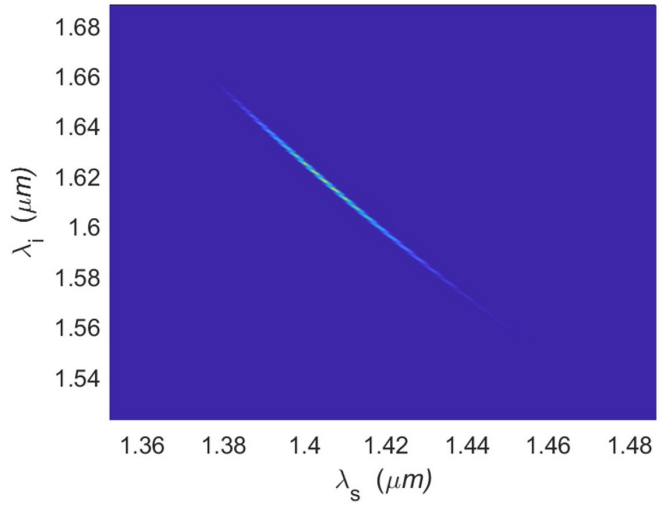

Figure 9: The resulting joint spectrum for this coupled waveguide geometry with an initial pulse duration $t_0 = 7ps$, a waveguide length of $L = 9000\mu m$ and a waveguide separation of $X = 420nm$.

$$J(\omega_i, \omega_s) = \sum_k \sqrt{b_k} u_k(\omega_s)\, v_k(\omega_i) \tag{16}$$

$$P = \frac{\sum b_k^2}{(\sum b_k)^2} \tag{17}$$

Photon purity can take any value from 0 to 1 where a photon purity of 1 indicates a pure heralded photon state. Here we see that using the device as described would yield highly correlated photon pairs with a purity $P = 16.7\%$. We can see for this set of geometry parameters, that the narrow bandwidth pump pulse and phasematching function overlap yielding a joint spectrum which indicates the generation of highly frequency correlated narrowband photons, with subsequently low photon purity.

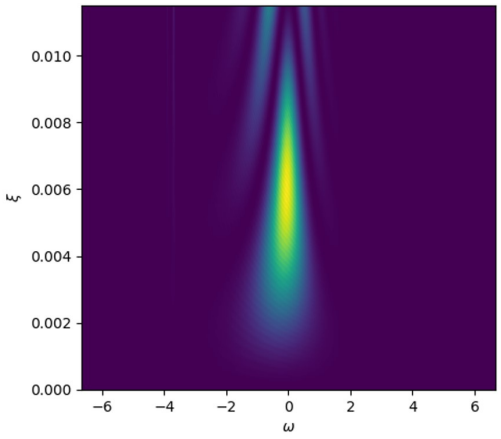

Figure 10: The resulting second harmonic in waveguide 2 with smaller initial pulse duration $t_0 = 6ps$, a waveguide length of $L = 9000\mu m$ and a waveguide separation of $X = 420nm$. "wings" are seen to enter the spectrum for this lower t_0.

For the phasematching function to be sufficiently narrow, the device length has to be increased. Increasing the length necessarily leads to the increase in the separation between the waveguides, such that a single oscillation in the pump field of waveguide 2 is observed. It was noticed, that for small

pulse duration the structure of the pump function in waveguide 2 was such that "wings" were observed emanating form the second oscillation of the pump field, shown in Fig. 10. The presence of these "wings" had an undesirable influence on the observed joint spectrum, and therefore a larger initial pulse duration was used to eliminate this. The consequence of having a narrow bandwith initial pulse is that the corresponding joint spectrum indicates highly frequency correlated narrowband photon generation.

2.4. Future work

Previous literature suggests that the result of our work is not surprising, as it has been reported that x-cut lithium niobate is more suitable for narrow band photon generation compared to z-cut geometries, which show the possibility for the generation of nearly frequency decorrelated states [23]. This thus motivates a direction for future work to involve the modelling of an analogous dual waveguide system with the modification of exchanging x-cut for z-cut lithium niobate, allowing for a full study of the effect this has on the generated photons. Additionally, it is ideal for photons to be generated closer to 1550nm for optimum integration with the pre-existing fibre technologies, since this wavelength corresponds to a minimum loss in standard telecoms fibre. Therefore, if the signal and idler could be generated at wavelengths closer to 1550nm and 1300nm respectively this would be of practical importance. One limitation to the approach outlined here is the generation of photons in the same spatial mode as this leads to symmetry in our phasematching function. Generation of photons in separate spatial modes, may allow for the lack of symmetry in the phasematching function to be utilised to yield less highly correlated photons, thus increasing photon purity by limiting the possible frequencies at which the signal and idler photons can be generated. Further to this continued computational analysis, it would be of significant interest to experimentally verify the behaviour and suitability of such devices, and to determine the viability of their application in quantum technologies.

Despite progress being made to improve the conversion rates and photon purity of photons generated through parametric down conversion processes [19, 25], the fundamental limitation of these sources remains. Their probabilistic nature and trade off between photon purity and high yield per pump pulse, due to high pumping powers leading to multiphoton emissions [19], will always be a fundamental physical limitation to these systems. Alternative avenues have been explored in recent years, with a promising deterministic alternative residing in the implementation of epitaxial quantum dots. These show promise, due to low rates of multiphoton emission and the potential for well defined emission characteristics [26]. Research is currently underway to realise C-band emission form such quantum dots through doping by ion implantation of Bismuth [27, 28].

3. Conclusions

Here we have presented the computational modelling and design of a novel and simplistic single photon source which, through the coupled processes of second harmonic generation and spontaneous parametric down conversion, is shown to generate highly correlated photons at wavelengths of about 1620nm and 1405nm with a photon purity of $P = 16.7\%$. Our results successfully demonstrate the potential to utilise phasematching between different modes in a coupled waveguide system as an alternative to periodic polling. However, for application as a heralded single photon source in quantum information processing, more work needs to be conducted. Specifically, in tuning the device to generate photons closer to $\lambda_{s,i} = 1550nm$ and exploring the possibility of using z-cut rather than x-cut lithium niobate as this may allow for the generation of frequency decorrelated photons with higher photon purity.

Acknowledgements

I would like to thank Dr Andriy Gorbach and Dr Peter Mosley for their supervision throughout this project, their guidance and feedback has been invaluable. I would also like to thank my project

partner Samuel Winter for his work and continued support. His script used to generate Fig. 8 and 10 can be found at: https://github.com/SamuelMBWinter/CoupledWaveguideFieldModel

References

[1] Georgescu, I M, Ashhab, S, and Nori, F 10, 2014. *Reviews of Modern Physics* **86** (1) 153–185.
[2] Maeda, K, Sasaki, T, and Koashi, M 17, 2019. *Nature Communications* **10** (1) 3140.
[3] Moreau, P-A, Toninelli, E, Gregory, T, and Padgett, M J 2019. *Nature Reviews Physics* **1** (6) 367–380.
[4] Azuma, K, Tamaki, K, and Lo, H-K 15, 2015. *Nature Communications* **6** (1) 6787.
[5] O'Brien, J L 7, 2007. *Science* **318** (5856) 1567–1570.
[6] DiVincenzo, D P and IBM 2000. *Fortschritte der Physik* **48** (9) 771–783.
[7] Smith, B J, Mahou, P, Cohen, O, Lundeen, J S, and Walmsley, I A 2009. *Conference on Lasers and Electro-Optics/International Quantum Electronics Conference*. International Quantum Electronics Conference. OSA ITuE2.
[8] Sharping, J E, Lee, K F, Foster, M A, Turner, A C, Schmidt, B S, Lipson, M, Gaeta, A L, and Kumar, P 11, 2006. *Optics Express* **14** (25) 12388–12393.
[9] Guo, X, Zou, C-l, Schuck, C, Jung, H, Cheng, R, and Tang, H X 2017. *Light: Science & Applications* **6** (5) e16249–e16249.
[10] Thomas, S and Senellart, P 2021. *Nature Nanotechnology* **16** (4) 367–368.
[11] Ngah, L A, Alibart, O, Labonté, L, D'Auria, V, and Tanzilli, S 2015. *Laser & Photonics Reviews* **9** (2) L1–L5.
[12] Boyd, R W 2003 *Nonlinear optics*. San Diego, CA: Academic Press.
[13] Shoji, I, Kondo, T, Kitamoto, A, Shirane, M, and Ito, R 1, 1997. *Journal of the Optical Society of America B* **14** (9) 2268.
[14] Wang, C, Zhang, M, Chen, X, Bertrand, M, Shams-Ansari, A, Chandrasekhar, S, Winzer, P, and Lončar, M 2018a. *Nature* **562** (7725) 101–104.
[15] Lin, J, Zhou, J, Wu, R, Wang, M, Zhiwei, F, Chu, W, Jianhao, Z, Qiao, L, and Sun, H 15, 2019. *Micromachines* **10** 612.
[16] Saravi, S, Pertsch, T, and Setzpfandt, F 2021. *Advanced Optical Materials* **9** (22) 2100789.
[17] Wang, C, Langrock, C, Marandi, A, Jankowski, M, Zhang, M, Desiatov, B, Fejer, M M, and Lončar, M 2018b. *Optica* **5** (11) 1438.
[18] Bock, M, Lenhard, A, Chunnilall, C, and Becher, C 17, 2016. *Optics Express* **24** (21) 23992–24001.
[19] Tang, J, Tang, L, Wu, H, Wu, Y, Sun, H, Zhang, H, Li, T, Lu, Y, Xiao, M, and Xia, K 8, 2021. *Physical Review Applied* **15** (6) 064020.
[20] Rowe, W R, Skryabin, D V, and Gorbach, A V 3, 2019. *Physical Review Research* **1** (3) 033146.
[21] Grice, W P and Walmsley, I A 1, 1997. *Physical Review A* **56** (2) 1627–1634.
[22] Main, P, Mosley, P J, Ding, W, Zhang, L, and Gorbach, A V 19, 2016. *Physical Review A* **94** (6) 063844.
[23] Ebers, L, Ferreri, A, Hammer, M, Albert, M, Meier, C, Förstner, J, and Sharapova, P R 2022. *Journal of Physics: Photonics* **4** (2) 025001.
[24] Yang, Z, Liscidini, M, and Sipe, J E 5, 2008. *Physical Review A* **77** (3) 033808.
[25] Cheng, X, Sarihan, M C, Chang, K-C, Lee, Y S, Laudenbach, F, Ye, H, Yu, Z, and Wong, C W 14, 2019. *Optics Express* **27** (21) 30773.
[26] Unitt, D C, Bennett, A J, Atkinson, P, Cooper, K, See, P, Gevaux, D, Ward, M B, Stevenson, R M, Ritchie, D A, and Shields, A J 2005. **7** (7) S129–S134.
[27] Cassidy, N, Blenkinsopp, P, Brown, I, Curry, R J, Murdin, B N, Webb, R, and Cox, D 2021. *physica status solidi (a)* **218** (1) 2000237.
[28] Marko, I P and Sweeney, S J 2017. *IEEE Journal of Selected Topics in Quantum Electronics* **23** (6) 1–12.